Cu-Zn Bimetallic Nanoparticles Decorated g-C_3N_4: A New-fashioned Electrochemical Sensing Application Designed for the Perception of Dopamine

A. Selvam[1], M. Sheik Muhideen Badhusha[1*], R.R. Muthuchudarkodi[2]

[1] Research department of chemistry, Sadakathullah Appa College, Tirunelveli-627011, Affiliated to Manonmaniam Sundaranar University, Abishekapatti, Tirunelveli-627012, Tamilnadu, India
[2] Research Department of chemistry, V.O. Chidambaram College, Thoothukudi-628008, TamilNadu, India
Corresponding Author: selvamsophiaphd@gmail.comdrbadhunano@gmail.com

Abstract:

In this study, we created a simple, low-cost material made of g-C_3N_4 adorned CuZn flower-shaped nanoparticles that was quickly produced in a single step using the hydrothermal process and had a large active surface area. UV-vis, FT-IR, XRD, SEM with EDX and HR-TEM spectral analyses and electrochemical techniques including Cyclic Voltammetry, Differential Pulse Voltammetry (DPV), and amperometry employed for sensor research were used to analyse and characterise g-C_3N_4 decorated CuZn. The UV-vis spectrum showed an absorption peak indicates the development of g-C_3N_4@CuZn Nps. The band gap energy of g-C_3N_4, CuZn bimetallic Nps and g-C_3N_4@CuZn Nps were 2.7 eV, 3.8 eV and 3.6 eV. FT-IR spectra for g-C_3N_4 showed sharp peak at 485 cm -1 and broad peak at 3542 cm-1 also gives further evidence to ensure the construction of g-C_3N_4 in CuZn bimetallic Nps. In XRD analysis of g-C_3N_4@CuZn Nps displays characteristic peaks located as 27.50 43.30, 50.40 can be indexed as a face centered cubic (fcc) structure. SEM images of pure g-C_3N_4 was layered structure, CuZn bimetallic Nps was Tremella-like structure, and g-C_3N_4@CuZn Nps was nano flower like structure.

Keywords: g-C_3N_4 decorated CuZn flower like nanoparticle, hydrothermal method, electrochemical sensor, Dopamine, Cyclic Voltammetry, amperometry.
DOI Number: 10.48047/NQ.2023.21.4.NQ23015 **Neuro Quantology 2023; 21(4): 145-159**

1. INTRODUCTION:

An essential neurotransmitter, dopamine (DA) affects the cardiovascular, central neurological, hormonal, and renal systems as well as the human metabolism [1]. Clinical and biochemical significance can be found in its qualitative and quantitative testing [2-4]. There have been a variety of methods that have been published throughout the years for the purpose of its measurement. Some of these methods include high-performance liquid chromatography [5], capillary electrophoresis [6], fluorescence [7], and electrochemical approach [8–9]. Because it could function well as an electron donor or hole scavenger [10] and demonstrated good sensitivity and selectivity, electrochemical sensors have recently been designed for measuring dopamine. [11-12]

One of the most important microelements, required for key processes, is zinc. The small intestine is where most of the zinc from food and water [13-15] that enters the body is absorbed. where it is deposited in proteins that accumulate zinc and cadmium [16], where it is bound by albumins and globulins. Zinc is a component of both hormone complexes and metalloenzymes. The ability of zinc to participate in the formation of ligands with organic molecules accounts for its widespread availability in various biological systems. Yet, because other cations that have accumulated in proteins can displace zinc, the distribution of zinc in tissues may alter. Zinc, for instance, is essential for many biological processes, including cell growth and division, keratogenesis, osteogenesis, immunological response, wound healing, including the healing of wounds from surgery, and pancreatic development and function.

Zinc, zinc ions, and zinc compounds' activities in the body as biomarkers and antioxidants [17], intravital and fatal distribution in tissues [18], action in particular structures (cell membranes, proteins, etc.), toxicity, and potential as therapeutic targets and biosensors have been researched recently. Zinc, a wurtzite-structured n-type semiconductor, is widespread. Due to its distinct physical and chemical characteristics, which can be used in a variety of applications including photocatalysts [19], optoelectronic devices, transducers, and sensors, Zn has recently gained increased attention. Zn has been demonstrated to be a superior gas sensitive material for the detection of both reducing and oxidising gases, and its gas sensing capabilities can be customised by doping or incorporating impurities [20].

Cu-Zn sensors exhibit exceptional sensitivity to numerous gases, including H2, CO, H2O, and Cl2, when compared to other doped Zn sensors [21]. The hetero contact between the p-type Cu and n-type Zn results in those superior sensing properties for Cu-Zn sensors [22]. It is implied that the chemical species to be detected in the environment may infiltrate through the interface of the p-n junction when the sensors are exposed to the target atmosphere, changing the electrical characteristics at the junction. Cu-Zn sensors have been the subject of numerous papers, but little research has been done on the sensing capabilities of Cu-Zn/CuO-ZnO nanoparticles (CZ/CZNs).

In order to assess the dopamine (DA) sensing capacities of carbon/Zn microfibers, Xiaowei and colleagues used a drop method. The suggested sensor was selective, repeatable, and stable, and had a detection limit of 0.106 M. Its detection limit was quite low. Dopamine catalysis may have been improved in the carbon/Zn-GCE because to its lower overpotential, smaller potential difference, and larger peak currents at 0.191/0.238 V. As copper particles have considerable bio affinities, high electron mobilities, and significant catalytic reactions, and hollow carbon spheres have a broad surface area and remarkable mass mobility, they are a good combination. The electrochemical detection of dopamine makes use of a number of nanomaterials based on ZnO. Zn and Cu metals because of the dopamine bio-affinity and selectivity of these elements.

In this study, we developed a single-step synthesis for g-C_3N_4, which has a high electron mobility and a low band gap. This technique offered a quick, easy, and inexpensive hydrothermal synthesis of a composite material that looked like a g-C_3N_4nanoflower and was ornamented with CuZn. The end product was a sensor with great selectivity and sensitivity to dopamine detection at room temperature without any further interference.

2. MATERIALS AND METHODS

2.1. Materials.

Several chemicals, including sodium borohydride ($NaBH_4$), ethanol (C_2H_6O), melamine ($C_3H_6N_6$), zinc sulphate heptahydrate ($ZnSO_4.7H_2O$), and copper (II) nitrate trihydrate (Cu $(NO_3)_2$ $3H_2O$, were purchased from Merck (Germany). Using water that has been through two distillation processes, nanoparticles were produced. All of the compounds were of an analytical

quality, and none of them were purified before use.

2.2. Methods for Synthesis

2.2.1. Fabrication of g-C_3N_4:

In order to produce graphitic carbon nitride, 550 degrees Celsius were maintained throughout the heating process of 10 grams of melamine for the duration of the first four hours. After being allowed to cool to room temperature, the fine yellowish powder of g-C_3N_4 was produced.

2.2.2. Fabrication of CuZn bimetallic Nanoparticle:

First, 0.5mm of Copper (II) Nitrate trihydrate (Cu $(NO_3)_2$ $3H_2O$) was dissolved in 50 mL of Double Distilled water (solution A). Second, 0.5 mm of Zinc sulfateheptahydrate ($ZnSO_4.7H_2O$) was added to a beaker to be dissolved in 40 mL of DD water (solution B). Next, solution B was slowly added to solution A (Adding solution A+B=solution C). Afterward, 0.01M of sodium borohydrate ($NaBH_4$) was dissolves in 5 ml of DD water adding into solution C in a dropwise manner under constant stirring. The pH was maintained at 11 by NaOH. The completed solution was transferred to an autoclave that had been lined with Teflon. The autoclave was then hermetically sealed and heated to 160 °C for 12 hours, which resulted in the production of a blueish solid substance. This material was then washed with double-distilled water and ethanol before being dried at 80 °C for 6 hours. The dry powder was then calcined at 450 degrees Celsius for three hours in order to generate CuZn bimetallic Nps.

2.2.3. Fabrication of g-C_3N_4 @CuZn Nanoparticle:

20 mL of double-distilled water and 50 mL of ethanol were combined with around 2g of the generated g-C_3N_4. Before adding 0.5mm of the CuZn bimetallic Nps sample, an ultrasonic probe sonicated the mixture for an hour. The mixture was sonicated for 2 h to form a homogeneous suspension before being moved to a Teflon-lined autoclave. The autoclave was sealed and heated to 120°C for three hours. The result was centrifuged, cleaned many times with double distilled water and ethanol, dried at 80oC for one hour, and then calcinated at 450oC for two hours. Finally, the black precipitate of g-C_3N_4@CuZn Nps was obtained.

2.3. Characterization.

Fourier Transmission JASCO FT-IR-4200 the functional group was analysed using infrared spectroscopy, and the absorbance of the newly formed nanoparticles was measured using a JASCO V-750 spectrophotometer. Using a D/max-RB diffractometer (Rigaku) and monochromatic Cu-K radiation, the XRD profiles of each sample were determined (0.1541 nm). The microstructure of the nanoparticles was examined using images captured with a TESCAN MIRA3 scanning electron microscope and a JOEL model 3010 HR-TEM.

3.RESULT AND DISCUSSION:

3.1. UV-Visible Spectroscopy:

In Figure 1 Shows the obvious absorption of g-C_3N_4, CuZn bimetallic Nps and g-C_3N_4@CuZn Nps. The optical residences and digital band systems of the synthesized bimetallic nanoparticles had been investigated with the aid of using UV-Vis spectroscopy. g-C_3N_4, CuZn bimetallic Nps and g-C_3N_4@CuZn Nps shows the absorption peaks at 365 nm, 326 nm, 344 nm. Using Tauc approach, energy band gap (E_g) for the above nanoparticles was calculated to be the bandgap values for the g-C_3N_4, CuZn bimetallic Nps and g-C_3N_4@CuZn Nps are 2.7 eV, 3.8 eV, 3.6 eV is confirmed in Figure 2. which is nicely matching with the literature values. The quantum confinement effect of smaller nanoparticles has the effect of widening the energy gap between the HOMO and LUMO states.

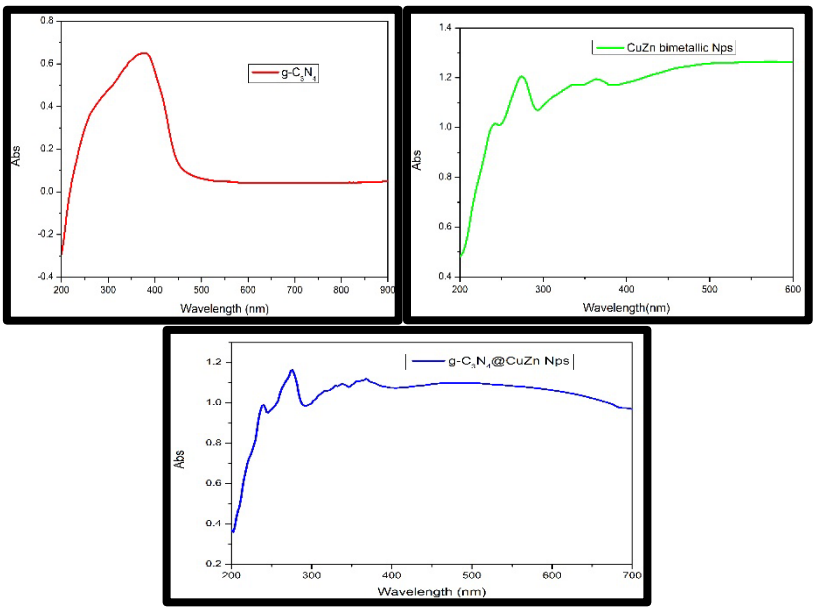

Fig. 1. UV-Visble Absorption spectra of g-C_3N_4, CuZn bimetallic Nps and g-C_3N_4@CuZn Nps

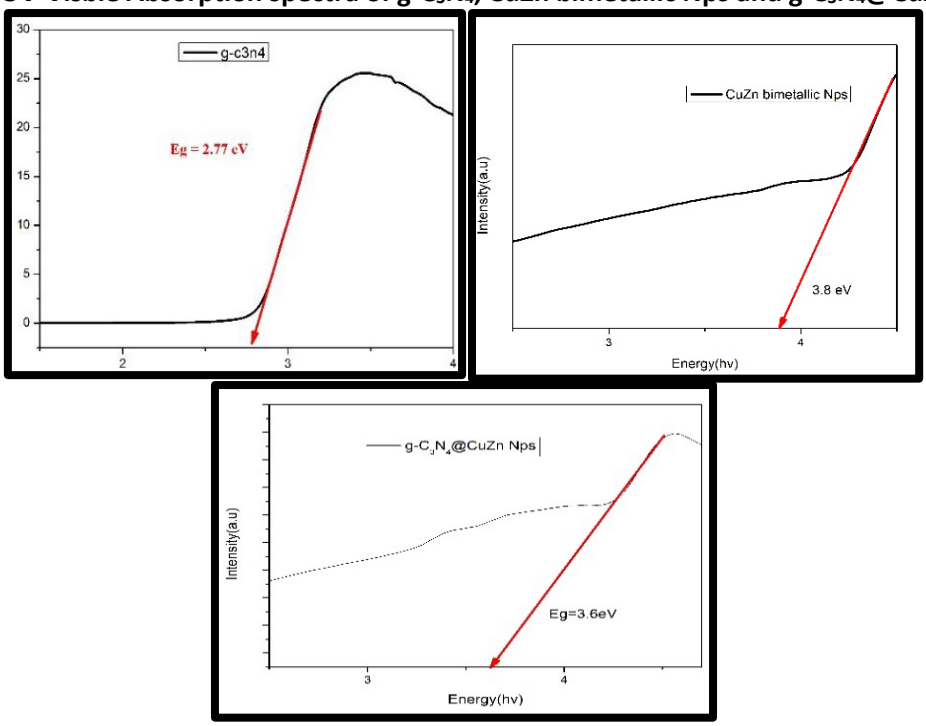

Fig. 2. Tauc Plots forg-C_3N_4, CuZn bimetallic Nps and g-C_3N_4@CuZn Nps

3.2. FT-IR:

The generated nanoparticles' FTIR spectra, which were acquired in the 400–4,000 cm-1 range, are shown in Figure 3. FTIR spectroscopy provides insight into the many functional groups and metal bonds present in nanoparticles. A significant vibration band seen at 485 cm-1 represents the typical stretching mode of CuZn bimetallic Nps. Two big peaks at 3542 cm-1 and 1280 cm-1 to 1470 cm-1 indicate the presence of an O-H functional group as a result of the nanoparticles' surface collecting moisture from the air.

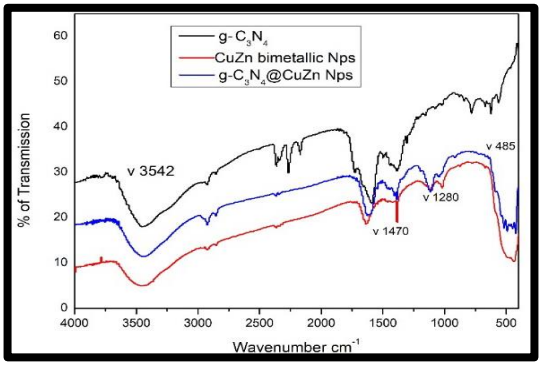

Fig. 3. FT-IR spectra of a) g-C_3N_4, CuZn bimetallic Nps and g-C_3N_4@CuZn Nps

3.3. XRD:

As-prepared samples of (a) g-C_3N_4, (b) CuZn bimetallic Nps, and (c) g-C_3N_4@CuZn Nps are shown in Figure 4. The peak of the X-ray diffraction pattern at 27.5 degrees indicated that g-C3N4 was a conventional graphite phase carbon nitride material without any additional impurity phases. CuZn bimetallic Nps' face-centered cubic phase. The face-centered cubic crystal planes (111), (200), and (002) are attributed to the diffraction peaks at 2= 38.4, 43.51, 48.3, 51.57, and 64.65. (220). The (100), (002), (101), (102), (110), (103) and (202) crystal planes and hexagonal crystal geometry of G-C_3N_4@CuZn bimetallic Nps, respectively, are represented by the diffraction peaks detected at 2 = 32.27, 34.10, 36.50, 46.40, 55.25, 62.12, and 77.72. (JCPSD card no. 01-007- 2551). Scherrer's equation, which is shown below, is used to calculate the average crystallite size (equation 1).

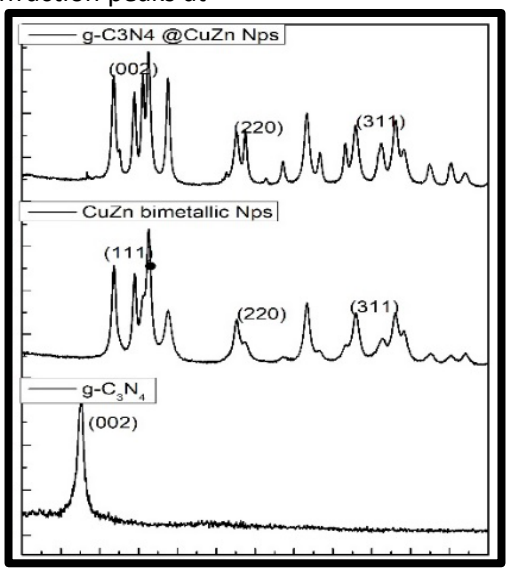

Fig. 4. XRD patterns of a) g-C_3N_4 b) CuZn bimetallic Nps and c) g-C_3N_4@CuZn Nps

$$D = \frac{K\lambda}{\beta \cos\theta} \quad (1)$$

Where β is the full width of half maximum of the peak, D is the average crystallite size. The X-ray incident angle is θ and wavelength is given by λ, whereas K is the particle shape factor (0.89). Crystallite diameters of g-C_3N_4, CuZn bimetallic Nps and g-C_3N_4@CuZn Nps were discovered for 19.6 nm, 30.1 nm, and 12.2 nm respectively. Particle size is decreases with increases of Dislocation density and Strain. The increased dislocation density and microstrain in g-C_3N_4@CuZn Nps signifies a decreased in number of defects in crystal lattice. The hallow carbon sphere have been shown in g-C_3N_4@Cuzn Nps have high surface area and great mass mobility properties and prominent high sensitivity. g-C_3N_4@CuZn Nps have low particle size and enhanced active surface area due to the nature of g-C_3N_4 doping with CuZn

bimetallic Nps, which in turn enable the high sensing activity towards dopamine.

Table 1. Comparison of g-C_3N_4, CuZn bimetallic Nps and g-C_3N_4@CuZn Nps with Particle size, Dislocation density and strain.

SAMPLE	PARTICLE SIZE $D=0.89\lambda/\beta Cos\ \theta$ (nm)	DISLOCATION DENSITY $P = 1/D^2$	STRAIN $\beta\ Cos\ \theta\ /4$
g-C_3N_4	19.6	0.0026	0.4243
CuZn bimetallic Nps	30.1	0.1078	0.0498
g-C_3N_4@CuZn Nps	12.2	0.6734	0.1163

3.4. SEM:

Figure 5 displays scanning electron micrographs of the CuZn bimetallic Nps decorated g-C3N4 nanoparticle with a nanoflower-like shape at different magnifications. Figure 5A shows the SEM images of pure g-C_3N_4 was layered structure, Fig 5B shows CuZn bimetallic Nps was Tremella-like structure, and Fig 5C shows g-C_3N_4@CuZn Nps was nano flower like structure. The Morphology was changing depending upon the nature of the g-C3N4 and CuZn bimetallic Nps.

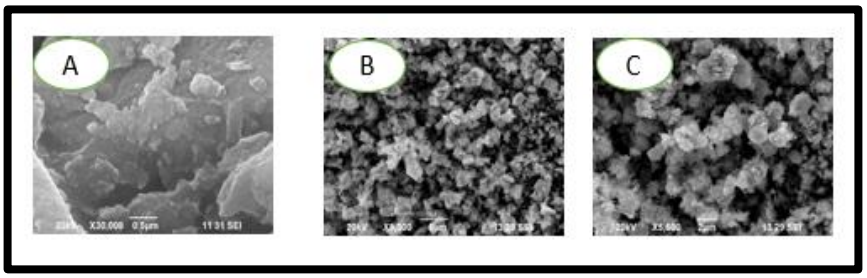

Fig. 5. SEM images for of (A) g-C_3N_4, (B) CuZn bimetallic Nps and (C) g-C_3N_4@Zn Nps

3.6. HR-TEM:

Figure 6 displays the morphological data for the g-C_3N_4@CuZn as well as the size distribution of the CuZn bimetallic Nps. As can be seen in the figure, the g-C_3N_4 material was characterised by a very irregular structure that was almost uniformly distributed throughout the substance. The aggregation of CuZnNps may account for the larger particle size of g-C_3N_4@CuZn Nps, which has a sphere-like shape.

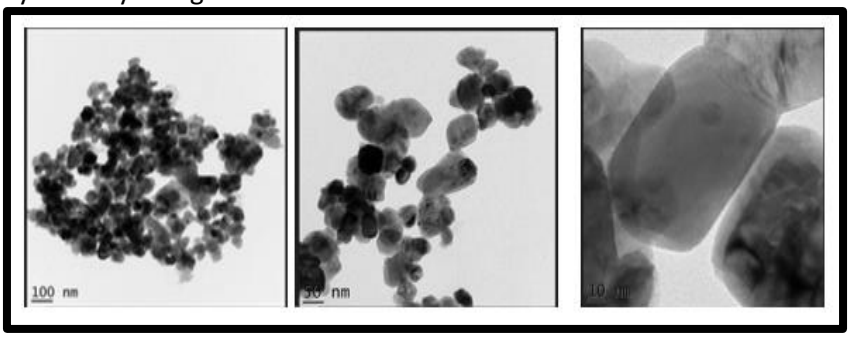

Fig. 8. HR-TEM images of g-C_3N_4@CuZn Nps

4. Electrochemical studies

CuZn/GCE and g-C_3N_4@CuZn/GCE bimetallic nanostructures were investigated by CV in 1 mM of $K_3[Fe(CN)_6]$ solution in 0.1 M of PBS (pH=7.0) for their electrocatalytic activity. Figure 9 displays a combined of well-defined redox curvature on the GCE. A two-electron and proton redox response has been realized owing to the sluggish electron transmission at the base GCE electrode, which exhibits the redox behaviour of Dopamine. A redox curve was found at

0.241 V and 1.813 V for g-C_3N_4 and a cathodic and anodic peak at 0.154 V and 1.81 V for CuZn/GCE severally. On one of these electrodes, the anodic peak current of g-C_3N_4@CuZn/GCE has been raised. Thus, g-C_3N_4@CuZn/GCE have an enormous surface area facilitates the transport of electrons between the two materials.

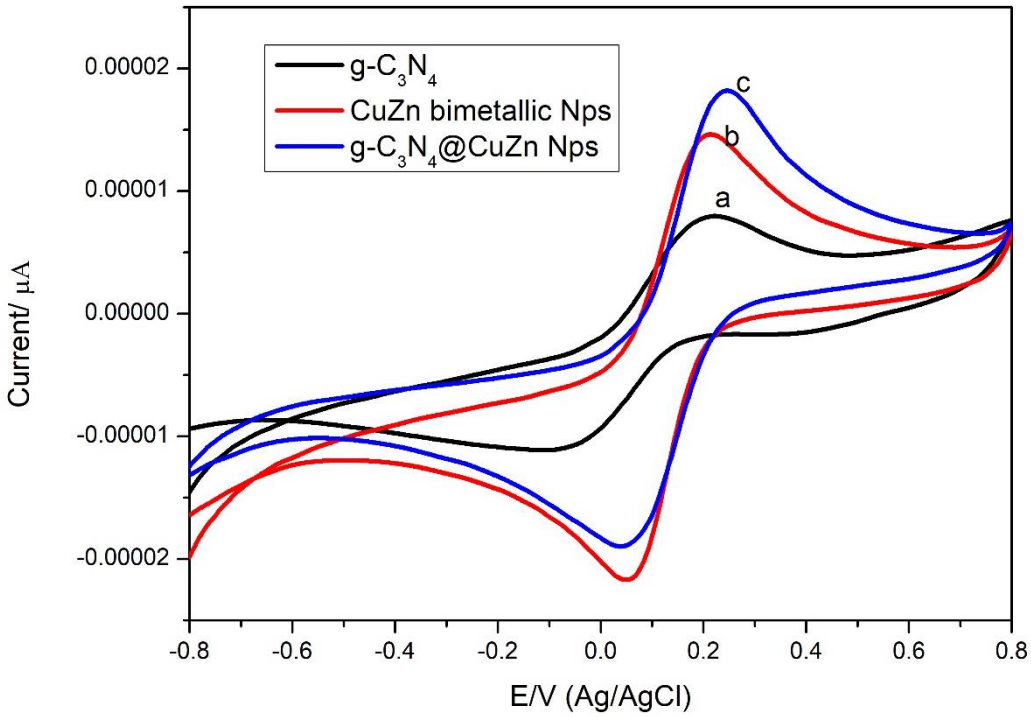

Fig. 9. CV curve of a) g-C_3N_4, b) CuZn/GCE and c) g-C_3N_4@CuZn/GCE in a 0.1 M PBS at 50 mV.s^{-1}.

4.1. Dopamine concentration, scan rate, and pH effect

Further, narrow down the range of possible Dopamine concentrations, the scan rate was increased to 50 mVs^{-1} while using the g-C_3N_4@CuZn/GCE method. Figure 10 shows the oxidation current, which ranges from +0.28 to +0.63 V. It is noticed that, the anodic curve shifts to the greater potential range as the Dopamine concentration increases. It is possible to achieve an electrode potential of 3.25 nA with the g-C_3N_4@CuZn/GC electrode for the Dopamine concentration of 10 µM. Figure 11 shows the related calibration plot disclosed the improved g-C_3N_4's efficiency toward Dopamine is demonstrated here together with the electrocatalytic capability of CuZn bimetallic Nps. Degradation of the modified electrode in repeated trials with the same electrode results in lower peak current at 12 mM Dopamine than at 10 mM Dopamine.

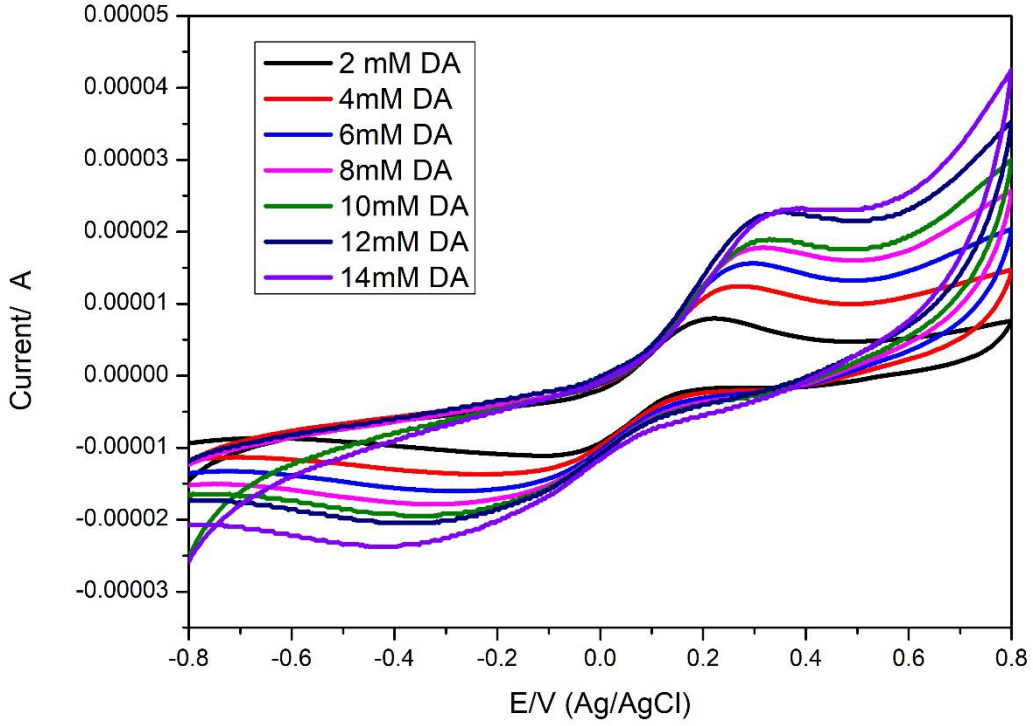

Fig. 10. CV curves of g-C_3N_4@CuZn/GCE under various Dopamine concentrations in a 0.1 mM PBS of 50 mV.s^{-1}.

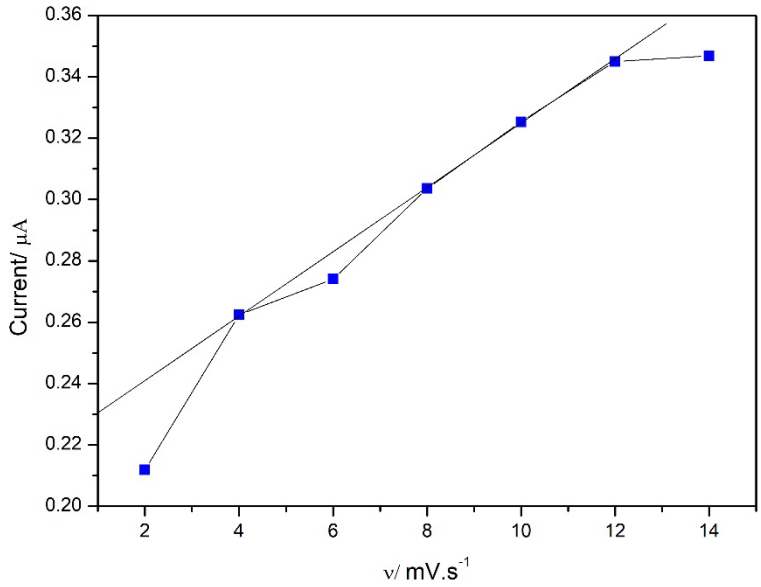

Fig. 11. Calibration plot between conc. of Dopamine and peak current

Scanning rates since 5 to 50 mV.s^{-1} are employed to observe the effect on peak currents and peak values of electrode reaction. The scan rate of cyclic voltammetry has a significant impact on Dopamine's oxidation peak current, as seen in Fig. 12. When the scan rate is increased, the biological compound's electrochemical oxidation peak potentials move positively. The increased conductivity of the modified electrode is thought to be due to the combination of CuZn bimetallic Nps with g-C_3N_4. As displayed in Fig. 13, a linear relationship exists between anodic potential and scan rate square root. That the electrode reactivity of this biological molecule has been affected by diffusion is revealed by these results.

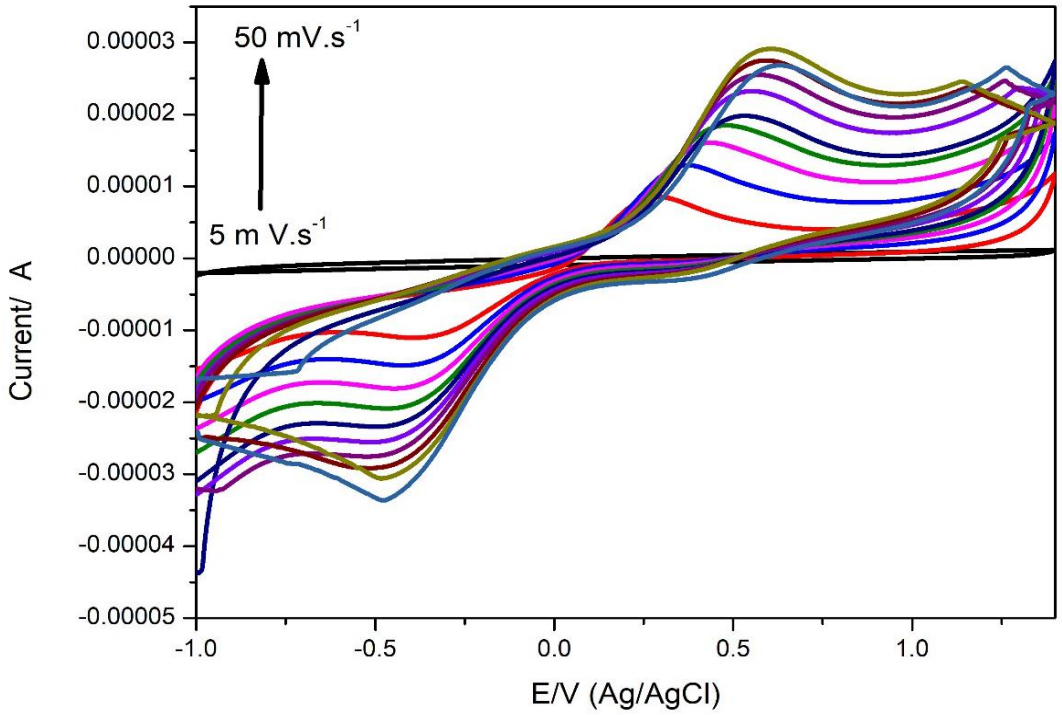

Fig. 12. Supporting CV of 0.1 mM dopamine in 0.1 M PBS at different scan rate, 5- 50 mV.s^{-1}.

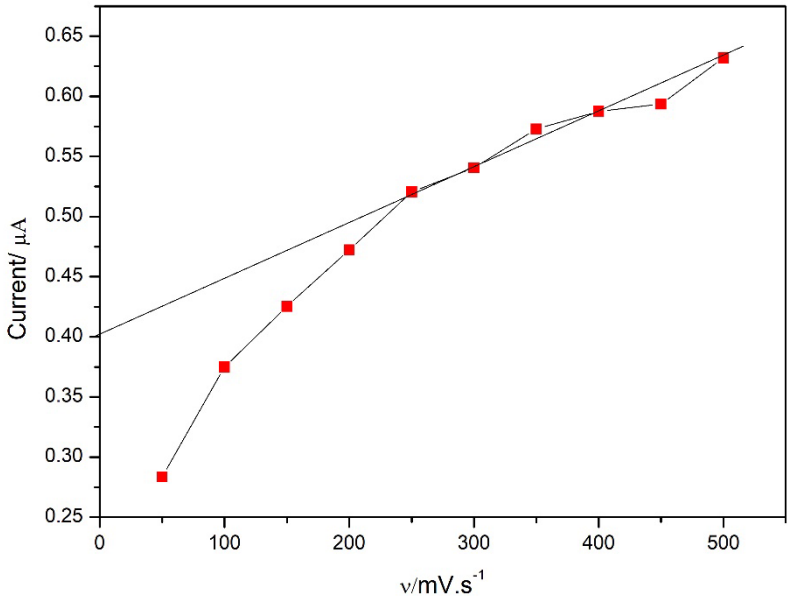

Fig. 13. The linear plot of anodic peak currents vs. scan rates.

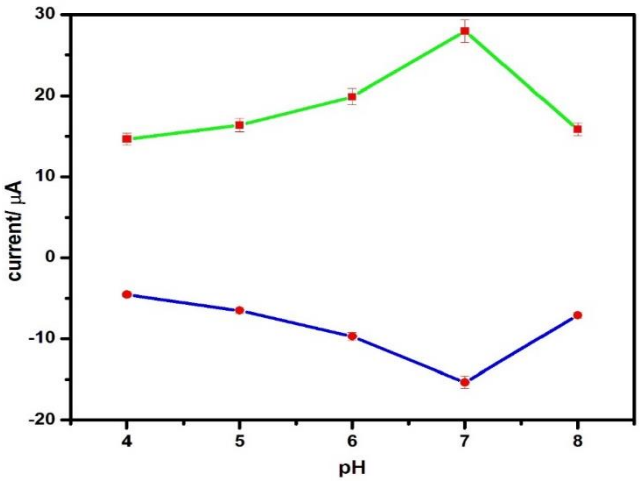

Fig. 14. Electrode potential of g-C_3N_4@CuZn/GCE plotted vs pH of 4-8.

According to Fig. 14, dopamine's electrochemical response was examined using CV in the pH of 4-8. Dopamine's anodic peak current climbed somewhat when the pH of the solution rose to 7.0. Dopamine's anodic peak potential, which occurs at pH 7, is wholly distinct from blood and urine pH values of 8 and below. In terms of pKa, dopamine has a value of 8.8. OH-ion participation is moderate between pH 4 and 7; at pH 7, OH-ion participation is substantial, hence the mode peak potential decreases. For electrochemical measurement of dopamine, the optimal pH is closer to pH = 7.

4.2 Evaluation of EIS

In EIS, the Nyquist plots reveal information about the electrode/solution interface parameters that have been adjusted on the electrode surface. Bare GCE, CuZn/GCE, and g-C_3N_4@CuZn/GCE are plotted in Fig. 15 against $[Fe(CN)_6]^{4-/3-}$ redox probe in the regularity sort of 0.01 Hz to 10 KHz in the Nyquist plot. Due to its tiny surface area for charge transfer, the bare GC electrode exhibits the biggest semicircle at large frequencies, which corresponds to its charge transmission resistance (Rct = 552.13). Using the Rct of Cu-Zn/GCE, a slighter semicircle with a charge transfer resistance of 157.35 ohms is shown. Furthermore, a smaller semicircle (Rct = 99.28) was observed in the g-C_3N_4@CuZn/GC modified electrode. This shows the large definite surface area and conductivity of g-C_3N_4 speed up electron transfer.

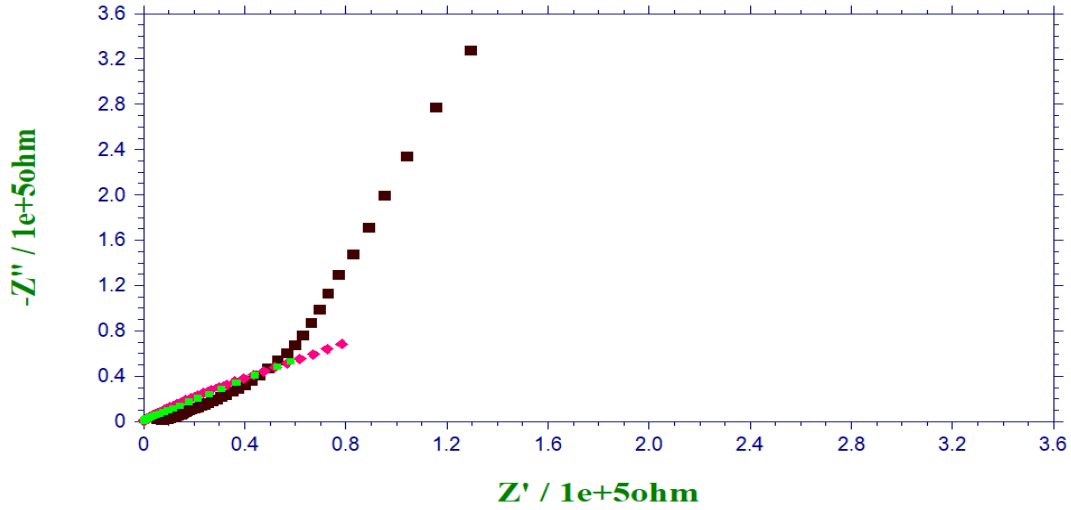

Fig. 15. Electrochemical impedance spectroscopy of bare GCE, CuZn bimetallic Nps/GCE and g-C_3N_4@CuZn/GCE in 0.1 M KCl containing 5.0 mM $[Fe(CN)_6]^{3-/4-}$.

4.3. Linear range of g-C_3N_4@CuZn/GCE

DPV was used to determine the Dopamine of g-C_3N_4@CuZn/GCE in order to explore its true linear range. Because DPV has an abundant greater current sensitivity and clever tendency than CV, it is a better choice. Scan rates of 50 mV.s^{-1} are used in Figure 16, show DPV responses at concentrations ranging from zero to three hundred (µM) (each one equal to 50 µM). Figure 17 illustrates the association between peak current and conc. of Dopamine. A linear increase in DPV current was seen as Dopamine concentration rose from 0 to 150 M.

Ipa(A) = 28.16 + 0.16 $C_{dopamine}$ is the linear region equation, and the correlation coefficient (R^2) is 0.9981. The results show that the g-C_3N_4@CuZn/GC electrode is more effective at electrochemically detecting Dopamine than previously reported electrodes. Comparison of present Dopamine sensor's results to those reported by former Dopamine sensors. For the dopamine sensor, the modified electrode g-C_3N_4@CuZn/GC electrode offers the best sensitivity, the widest linear range, the lowest detection limit and fastest detection time.

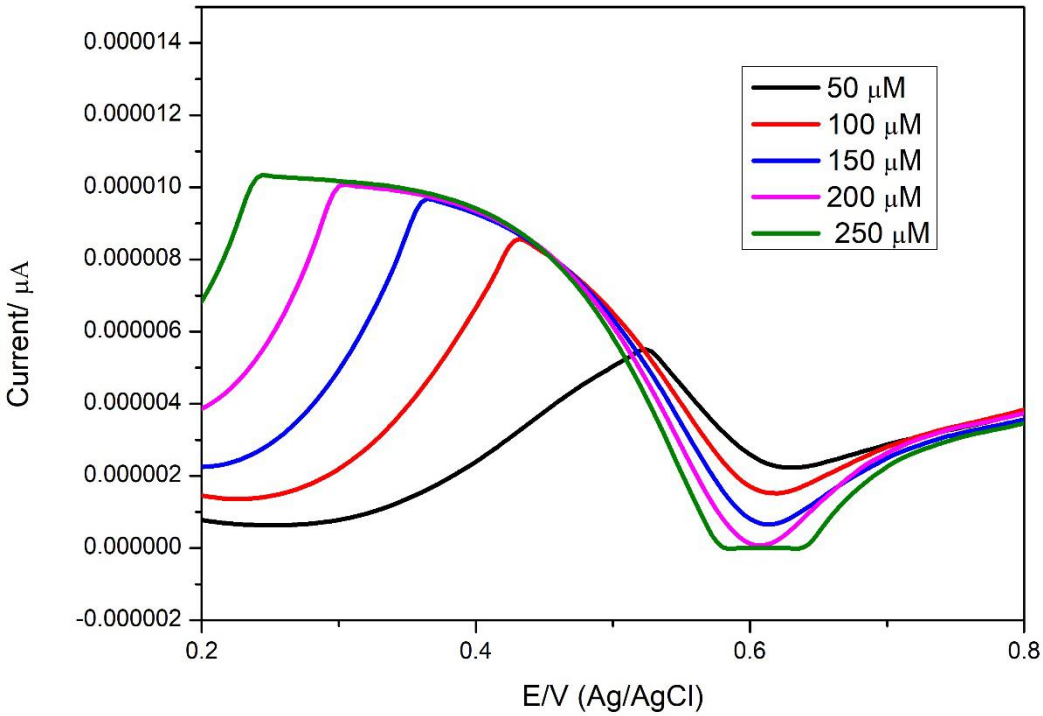

Fig. 16. DPV response of g-C_3N_4@CuZn/GCE biosensor with the range of 0 to 300 µM of Dopamine in 0.1 M of PB solution at the scan rate of 50 mV.s^{-1}.

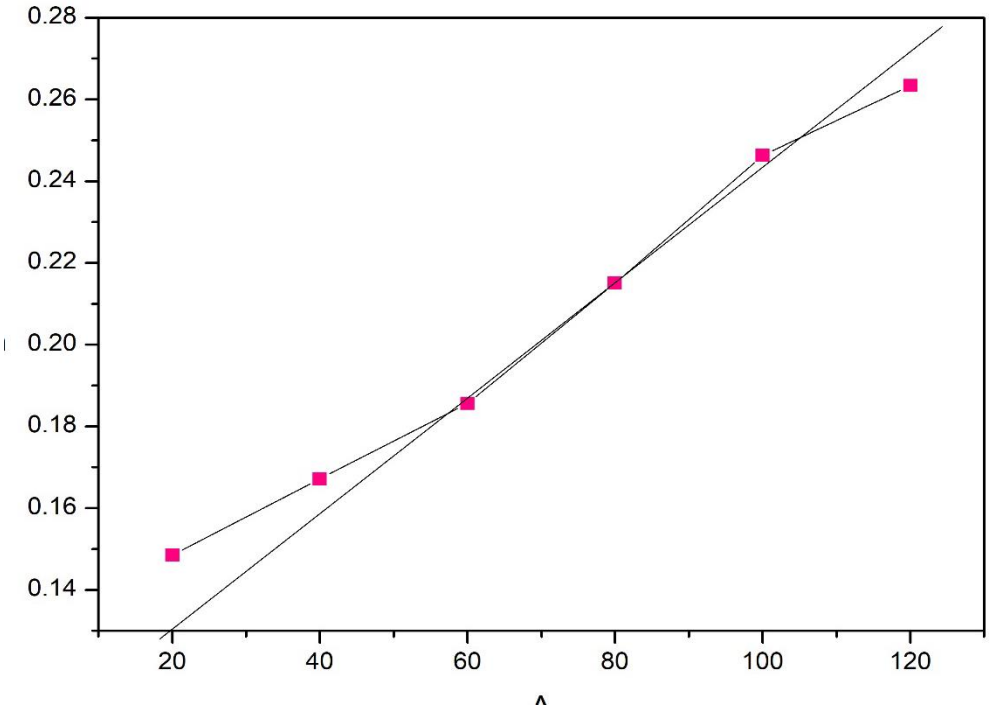

Fig. 17. Corresponding calibration plot between current and conc. of Dopamine

4.4. Consistency and repeatability

The electrochemical sensor's performance is mostly evaluated based on the sensor's stability and reproducibility. Electrode CVs were obtained for 0.5 µM of Dopamine in 0.1 M PBS (pH=7) using g-C_3N_4**@**CuZn/GC modified electrode. A comparative standard deviance of 1.4% and 1.2% was observed in the oxidation peak current of Dopamine for 20 repetitions of the experiment. The current signal of g-C_3N_4**@**CuZn/GCE sensors was measured with an RSD of -- percent to test the repeatability of the changed electrodes. Based on these findings, it appears that the reformed electrode could serve a sensitive and selective Dopamine sensor that is stable and has high sensitivity.

4.7. Consistency and repeatability

The performance of an electrochemical sensor is primarily assessed based on its stability and repeatability. Using a g-C3N4@CuZn/GC modified electrode, electrode CVs for 0.5 M of dopamine in 0.1 M PBS (pH=7) was obtained. For 20 iterations of the experiment, a comparable standard deviation of 1.4% and 1.2% was seen in the dopamine oxidation peak current. To check the repeatability of the new electrodes, the current signal of g-C3N4@CuZn/GCE sensors was measured with an RSD of percent. Based on these results, it would seem that the reformed electrode could function as a very sensitive and stable dopamine sensor.

4.8. Analysis of a real sample

Male patients at the Madurai Medical College Hospital in Madurai were asked to provide urine samples for testing. Dopamine analysis began with a 10-fold dilution of the urine sample. The conventional addition method was used to measure the DA. Table 4 displays the findings. Because dopamine is present in biological samples, or because of complicated matrix effects, all samples show a recovery of higher than 100%. This shows that g-C_3N_4**@**CuZn/GCE sensors are appropriate and selective for the measurement of DA in living samples because the recovery was very adjacent to 100%. This reveals the brilliant selectivity of g-C_3N_4**@**CuZn/GCE sensors of DA in natural samples.

Table 4. Determination of DA in human urine samples using g-C_3N_4@CuZn/GCE sensor (Practical application of the proposed method n = 3)

Urine Sample	Added (µM)	Found (µM)	RSD (%)	Recovery (%)
A	5	4.02	2.77	98.05
B	5	4.28	2.72	98.82
C	5	4.19	2.39	98.59
D	5	4.51	1.95	99.12
E	5	4.67	2.29	99.34

5. Conclusion

The structure of the Cu-Zn-modified g-C_3N_4 is examined by several spectrum analyses. The CuZn bimetallic Nps structure belongs to the family of hexagonal structures. SEM g-C_3N_4@CuZn picture reveals a layered structure with a rough surface resembling a sphere. As a DA sensor, g-C_3N_4@CuZn nanoparticle is used. The g-C_3N_4@CuZn nanoparticle was tailored to the GCE surface for the electrochemical resolution of DA. The graphene and g-C_3N_4@CuZn nanoparticle combination significantly improves the oxidation peak current of DA. Because to the synergistic qualities of graphene's remarkable capacity and the increased electronic conductivity of the g-C_3N_4@CuZn nanoparticles, the intriguing electrocatalytic activity of g-C_3N_4@CuZn to DA was possible. Noble sensitivity, selectivity, stability, reproducibility, and a low detection limit are all characteristics of the g-C_3N_4@CuZn reformed GCE. The outstanding achievement of fabricated sensor was validated for the detection of DA in real samples of adequate results.

References:

1. Bernardo-Bermejo S, Sanchez-Lopez E, Castro-Puyana M, Marina ML. Chiral capillary electrophoresis. TrAC Trends in Analytical Chemistry. 2020; 124:115807.
2. Bucolo C, Leggio GM, Drago F, Salomone S. Dopamine outside the brain: The eye, cardiovascular system and endocrine pancreas. Pharmacology & Therapeutics. 2019; 203:107392.
3. El-Bahr SM, Shousha S, Albokhadaim I, Shehab A, Khattab W, Ahmed-Farid O, El-Garhy O, Abdelgawad A, El-Naggar M, Moustafa M, Badr O. Impact of dietary zinc oxide nanoparticles on selected serum biomarkers, lipid peroxidation and tissue gene expression of antioxidant enzymes and cytokines in Japanese quail. BMC veterinary research. 2020;16(1):1-2.
4. Ferré S, Ciruela F, Woods AS, Lluis C, Franco R. Functional relevance of neurotransmitter receptor heteromers in the central nervous system. Trends in neurosciences. 2007;30(9):440-6.
5. Ganiyu SO, Martinez-Huitle CA, Rodrigo MA. Renewable energies driven electrochemical wastewater/soil decontamination technologies: A critical review of fundamental concepts and applications. Applied Catalysis B: Environmental. 2020;270:118857.
6. Glauner B. Separation and quantification of muropeptides with high-performance liquid chromatography. Analytical biochemistry. 1988;172(2):451-64.
7. Hayes R, Ahmed A, Edge T, Zhang H. Core–shell particles: Preparation, fundamentals and applications in high performance liquid chromatography. Journal of chromatography A. 2014; 1357:36-52.

eISSN1303-5150

8. He C, Tao M, Zhang C, He Y, Xu W, Liu Y, Zhu W. Microelectrode-based electrochemical sensing technology for in vivo detection of dopamine: recent developments and future prospects. Critical Reviews in Analytical Chemistry. 2022;52(3):544-54.
9. Ibuot A, Webster RE, Williams LE, Pittman JK. Increased metal tolerance and bioaccumulation of zinc and cadmium in Chlamydomonasreinhardtii expressing a AtHMA4 C-terminal domain protein. Biotechnology and Bioengineering. 2020;117(10):2996-3005.
10. Jeon YR, Yu J, Choi SJ. Fate determination of ZnO in commercial foods and human intestinal cells. International Journal of Molecular Sciences. 2020;21(2):433.
11. Lacasa E, Cotillas S, Saez C, Lobato J, Cañizares P, Rodrigo MA. Environmental applications of electrochemical technology. What is needed to enable full-scale applications. Current Opinion in Electrochemistry. 2019; 16:149-56.
12. Lakshmanakumar M, Nesakumar N, Kulandaisamy AJ, Rayappan JB. Principles and recent developments in optical and electrochemical sensing of dopamine: A comprehensive review. Measurement. 2021; 183:109873.
13. Liu R, Feng ZY, Li D, Jin B, Lan Y, Meng LY. Recent trends in carbon-based microelectrodes as electrochemical sensors for neurotransmitter detection: A review. TrAC Trends in Analytical Chemistry. 2022:116541.
14. Mnethu O, Nkosi SS, Kortidis I, Motaung DE, Kroon RE, Swart HC, Ntsasa NG, Tshilongo J, Moyo T. Ultra-sensitive and selective p-xylene gas sensor at low operating temperature utilizing Zn doped CuOnanoplatelets: Insignificant vestiges of oxygen vacancies. Journal of Colloid and Interface Science. 2020; 576:364-75.
15. Mohammadi H, Talebi S, Ghavami A, Rafiei M, Sharifi S, Faghihimani Z, Ranjbar G, Miraghajani M, Askari G. Effects of zinc supplementation on inflammatory biomarkers and oxidative stress in adults: A systematic review and meta-analysis of randomized controlled trials. Journal of Trace Elements in Medicine and Biology. 2021; 68:126857.
16. Moreno-Olivas F, Tako E, Mahler GJ. ZnO nanoparticles affect nutrient transport in an in vitro model of the small intestine. Food and Chemical Toxicology. 2019; 124:112-27.
17. Ouedraogo S, Meunier-Prest R, Kumar A, Bayo-Bangoura M, Bouvet M. Modulating the electrical properties of organic heterojunction devices based on phthalocyanines for ambipolar sensors. ACS sensors. 2020;5(6):1849-57.
18. Prabhu K, Malode SJ, Shetti NP, Kulkarni RM. Analysis of herbicide and its applications through a sensitive electrochemical technique based on MWCNTs/ZnO/CPE fabricated sensor. Chemosphere. 2022; 287:132086.
19. Qian W, Xu S, Zhang X, Li C, Yang W, Bowen CR, Yang Y. Differences and similarities of photocatalysis and electrocatalysis in two-dimensional nanomaterials: strategies, traps, applications and challenges. Nano-Micro Letters. 2021; 13:1-38.
20. Sohal IS, DeLoid GM, O'Fallon KS, Gaines P, Demokritou P, Bello D. Effects of ingested food-grade titanium dioxide, silicon dioxide, iron (III) oxide and zinc oxide nanoparticles on an in vitro model of intestinal epithelium: Comparison between monoculture vs. a mucus-secreting coculture model. NanoImpact. 2020; 17:100209.
21. Wang CN, Li YL, Gong FL, Zhang YH, Fang SM, Zhang HL. Advances in doped ZnO nanostructures for gas sensor. The Chemical Record. 2020;20(12):1553-67.
22. Wei X, Zhang Z, Wang Z. A simple dopamine detection method based on fluorescence analysis and dopamine polymerization. Microchemical Journal. 2019; 145:55-8.
23. Zhang F, Yang L, Bi S, Liu J, Liu F, Wang X, Yang X, Gan N, Yu T, Hu J, Li H. Neurotransmitter dopamine applied in electrochemical determination of aluminum in drinking waters and

biological samples. Journal of Inorganic Biochemistry. 2001 Nov 1;87(1-2):105-13.

24. Zheng C, Li B, Hong C, Peng A, Chen X. Chitosan as a promising hole-scavenger for photoelectrochemical monitoring of water cobalt (II) ions. Journal of Electroanalytical Chemistry. 2019; 851:113470.
25. Zhou J, Del Rosal B, Jaque D, Uchiyama S, Jin D. Advances and challenges for fluorescence nanothermometry. Nature methods. 2020;17(10):967-80.